ACS EARTH AND SPACE CHEMISTRY

http://pubs.acs.org/journal/aesccq

Article

Transformation of Ferrihydrite to Goethite and the Fate of Plutonium

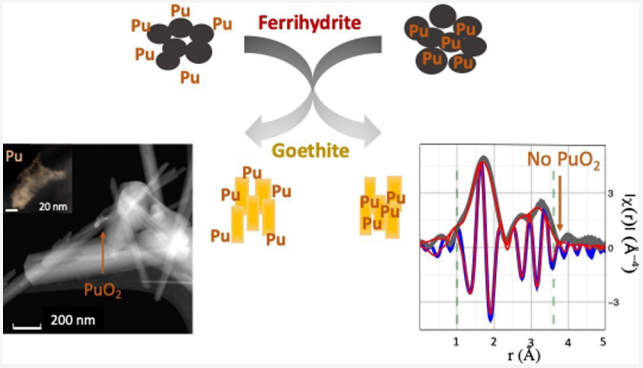
Enrica Balboni,* Kurt F. Smith, Liane M. Moreau, Tian T. Li, Melody Maloubier, Corwin H. Booth, Annie B. Kersting, and Mavrik Zavarin

Cite This: *ACS Earth Space Chem.* 2020, 4, 1993−2006

Read Online

ACCESS | Metrics & More | Article Recommendations | Supporting Information

ABSTRACT: Understanding the interactions between plutonium and iron (oxy)hydroxide minerals is necessary to gain a predictive understanding of plutonium environmental mobility and to evaluate long-term performance of nuclear waste repositories. We investigated the fate of plutonium during the formation of ferrihydrite and its subsequent transformation into goethite. Ferrihydrite was synthesized with varying quantities of Pu(IV) following either a sorption or coprecipitation process; the ferrihydrite was then aged hydrothermally to yield goethite. The synthesized materials were characterized via extended X-ray absorption fine structure spectroscopy, transmission electron microscopy, and acid leaching to elucidate the nature of plutonium association with ferrihydrite and goethite. In samples prepared following the sorption method, plutonium was identified in two different forms: a PuO_2 precipitate and a surface-sorbed plutonium complex. For the samples prepared via coprecipitation, no PuO_2 formation occurs in the ferrihydrite precursor and in the goethite experiments where plutonium concentration is ≤1000 ppm (mg kg^{-1}). In these coprecipitation products, plutonium is strongly bound to the minerals either via formation of an inner sphere complex, or via an incorporation process. In the coprecipitation experiments, PuO_2 formation only occurs at the highest plutonium concentration (3000 ppm), suggesting that during ferrihydrite transformation into goethite, part of the plutonium can be remobilized to form PuO_2 nanoparticles. Collectively, our results demonstrate that the nature of plutonium associated with the precursor ferrihydrite (adsorbed vs coprecipitated) will have a direct impact on the association of plutonium with its alteration product (goethite). Furthermore, the data illustrate that some properties of plutonium association with the precursor ferrihydrite are retained through the transformation into goethite. These findings show that plutonium strongly associates with iron (oxy)hydroxides formed through coprecipitation processes and in these materials, plutonium can be strongly retained by the iron minerals.



KEYWORDS: *ferrihydrite, goethite, plutonium, extended X-ray absorption fine structure spectroscopy*

Downloaded via LOS ALAMOS NATL LABORATORY on September 3, 2025 at 19:48:02 (UTC).
See https://pubs.acs.org/sharingguidelines for options on how to legitimately share published articles.

INTRODUCTION

The production and testing of nuclear weapons, nuclear accidents, and authorized discharges of radioactive effluents have contributed significantly to plutonium (Pu) contamination in the natural environment. Pu is also a major constituent in civil and military nuclear wastes and is considered a risk-driving radionuclide in the long-term safety of nuclear waste repositories. Because of its long half-life (^{239}Pu $t_{1/2}$ = 24,100 years) and radiotoxicity, understanding the mobility of Pu in the environment is a key scientific and societal concern.

Several factors can influence Pu mobility in the environment including: Pu redox processes,[1−3] solubility effects,[4,5] interactions with natural organic matter (including bacteria),[6,7] and sorption/desorption reactions with mineral surfaces.[8−10] Under typical environmental conditions, Pu may exist in the III, IV, V, and/or VI oxidation states, each of which demonstrates dramatically different chemical properties.[11,12]

For example, under environmental conditions, the higher oxidation states, V and VI, exist as the highly soluble and mobile PuO_2^{x+} moieties. Although Pu(V) and Pu(VI) predominate under oxic conditions, Pu(IV) is often the most common plutonium ion at neutral pH and under mildly reducing conditions.[13] Pu(IV) undergoes rapid hydrolysis in circumneutral environments resulting in a significantly lower solubility than the higher oxidations states, V and VI. Pu

Received: July 16, 2020
Revised: September 22, 2020
Accepted: October 9, 2020
Published: October 27, 2020



ACS Publications

© 2020 American Chemical Society

hydrolysis reactions may occur at Pu(IV) concentrations $>10^{-8}$ M[14] and result in the formation of discrete $[Pu(OH)_n]^{(4-n)^+}$ intrinsic colloids.[5,13,15−19] At pH > 3, the Pu aqueous concentration is dominated by Pu(V) and by the solubility product of the Pu(IV) hydrous oxide precipitate. Although Pu(IV) and Pu(V) are the most common oxidation states under circumneutral pH conditions, and both sorb to Pu mineral surfaces, Pu(V) has been shown to reduce to Pu(IV) on surfaces.[2,8,11,20−23] Moreover, Pu(IV) has a particularly high affinity for iron (oxy)hydroxide mineral surfaces.[2,24,25] Iron (oxy)hydroxides are a common constituent of soils, and predominantly form as alteration products of iron-bearing minerals.[26] In the deep subsurface, iron (oxy)-hydroxides may form because of biological oxidation of Fe(II) under reducing conditions.[27] Fe minerals in transient and dynamic (bio)geochemical settings such as sediment deposition in lakes or ponds[28−30] will likely be subject to dissolution and phase transformation reactions,[2,24,31,32] and the fate of the sorbed species during these processes is currently unknown. In nuclear repositories planned by several countries, the first technical containment barrier planned for use consists of stainless-steel canisters.[33−35] Under nuclear repository conditions, the steel cask is expected to corrode over the geological timescales considered[33−35] and depending on the engineered backfill material, the natural bedrock, and the nature of surrounding groundwater, a range of Fe minerals may form during the corrosion process.[36,37]

Ferrihydrite ($Fe_{9.74}O_{14}(OH)_2$, FH)[38] is a poorly crystalline and metastable early product of both biotic and abiotic precipitation of iron, and is a precursor to more crystalline iron oxide phases such as hematite (α-Fe_2O_3) and goethite (α-FeOOH, goethite). Ferrihydrite transformation into either hematite or goethite has been well studied and is strongly dependent upon solution conditions, including pH, ionic strength, and temperature.[39−44] Ferrihydrite typically exhibits a high surface area with a high capacity to adsorb dissolved metal species,[45−47] including U, Np, and Pu.[26,48−51] These traits of ferrihydrite have been utilized to decontaminate radioactive effluents[52] and in various nuclear abatement technologies.[53]

When Pu is present in solutions where iron (oxy)hydroxide minerals may be forming, such as in contaminated ponds, lakes, or streams, or during corrosion of steel, its fate is unknown. Pu could conceivably adsorb to the newly formed iron oxides (e.g., hematite or goethite), be structurally incorporated into the new phases, or be excluded from the newly formed crystal structure because of the crystal-chemical constraints. These three different scenarios have vastly different implications for predicting contaminant transport. Smith et al.[48] demonstrated that under high pH conditions (pH 9), Pu forms an inner-sphere tetradentate complex on the ferrihydrite surface,[48] which remains unchanged during transformation into hematite, suggesting that Pu remains strongly adsorbed to the iron (oxy)hydroxide surface[48] during hematite crystallization. Recent experiments by Marshall et al. (2014)[26] and Bots et al. (2016)[49] showed that U(VI) and Np(V) initially adsorbed to ferrihydrite can be incorporated into a distorted Fe(III) octahedral site in the hematite structure during phase transformation.[26,49] The transformation of ferrihydrite into nanoparticulate iron (oxy)hydroxide minerals in the presence of U(VI) resulted in the preferential incorporation of U into goethite (α-FeOOH) over lepidocrocite (γ-FeOOH).[54] At high Pu concentrations ($>10^{-8}$ M), Pu(IV) intrinsic colloids have been shown to form on the surface of various oxide minerals including iron oxy-(hydroxide) minerals.[15,24,55,56] On the goethite surface, Pu(IV) colloids may undergo a lattice distortion, because of epitaxial growth, which leads to a stronger surface binding compared to other mineral phases, such as quartz.[15] Both the sorption/desorption of Pu to mineral colloid surfaces (pseudocolloids) and formation of Pu oxide colloids (intrinsic colloids) associated with mineral surfaces, as well as Pu coprecipitation with secondary minerals are all likely important environmental processes under a range of geochemical conditions.[11,14,22,57,58] For example, in groundwater at the Mayak site (Russia), colloidal amorphous iron oxides with associated Pu were found up to 4 km away from the contamination source.[59] In contaminated soils at Los Alamos National Laboratory, Batuk et al.[60] identified unusual Pu−Fe particles. The authors suggest that the formation of these particles could have resulted from transitory local chemical conditions from the original waste stream.[60] Finally, Lukashenko et al. (2020)[61] identified particles of Pu containing Fe−Mn oxides in bottom sediments of streams flowing from the tunnels in the Degelen Mountain, a site of the USSR nuclear weapon testing program.[61] Analysis of the particles indicates that these materials may be formed as secondary minerals, suggesting that their formation is most likely related to sorption and coprecipitation of transuranic elements with oxides and hydroxides of iron and manganese.[61]

The fate of radionuclides, including Pu, during mineral formation and crystallization processes is still not fully understood. Gaining a detailed, mechanistic, understanding of the interactions between iron (oxy)hydroxides and Pu is key to predicting the long-term stability and mobility of Pu in the natural and engineered environment. The goal of this work is to assess the fate of Pu during the ubiquitous process of ferrihydrite into goethite transformation. We synthesized ferrihydrite with various amounts of Pu(IV) following either a coprecipitation or sorption process, and then subsequently used this material to crystallize goethite. We provide detailed extended X-ray absorption fine structure spectroscopy (EXAFS) and transmission electron microscopy (TEM) characterization of the synthesized minerals and show that the nature of Pu associated with the precursor ferrihydrite (adsorbed vs coprecipitated) will impact the association of Pu with the ferrihydrite alteration product (goethite).

METHODS

Preparation of Pu Stock. A ^{242}Pu stock (99.8% ^{242}Pu, 0.12% ^{240}Pu, 0.005% ^{239}Pu, and 0.005% ^{238}Pu by activity) was purified using an anion exchange resin (BioRad AG1-X8, 100−200 mesh). Prior to loading on the resin, Pu was reacted with $NaNO_2$ to convert Pu to Pu(IV). Pu was loaded onto the column in 8 mol/L HNO_3 and the column was subsequently washed with three column volumes of 8 mol/L HNO_3. Pu was stripped from the column using 1 mol/L HCl. The oxidation state of Pu was determined using the lanthanum fluoride precipitation method[62] and determined to be 97% Pu(III/IV). UV−vis confirmed that the Pu stock solution was >95% Pu(IV). The concentration of the purified stock solution was determined by liquid scintillation counting (LSC; Packard Tri-Carb TR2900 LSA) with final a concentration of $1.3 \pm 0.1 \times 10^{-3}$ mol/L.

https://dx.doi.org/10.1021/acsearthspacechem.0c00195
ACS Earth Space Chem. 2020, 4, 1993−2006

Mineral Synthesis. *Ferrihydrite Sorption Method.* Ferrihydrite precipitation was induced by dropwise addition of 1−5 mol/L KOH into a 25 mL 0.04 mol/L $FeNO_3{\cdot}9H_2O$ solution in 30 mL Savillex perfluoroalkoxy alkane (PFA) vials to yield a final pH ∼ 8. Desired aliquots of a Pu(IV) stock solution were added to the mineral slurries. After addition of the Pu(IV) stock, the pH of the slurries was checked and readjusted to the desired value using 1−5 mol/L KOH. The FH−Pu(IV) suspensions were equilibrated for 2 h. Samples prepared following this sorption method with 3000, 1000, and 400 ppm Pu(IV) will be referred to as FH_S-3000, FH_S-1000, and FH_S-400, respectively.

Ferrihydrite Coprecipitation Method. A 25 mL 0.04 mol/L $FeNO_3{\cdot}9H_2O$ solution was mixed with desired concentrations of Pu(IV). The solutions were equilibrated for 2 h in 30 mL Savillex PFA vials. Ferrihydrite precipitation was induced by dropwise addition of 1−5 mol/L KOH to a final pH of ∼8 and samples with 3000, 1000, and 400 ppm Pu(IV) will be referred to as FH_C-3000, FH_C-1000, and FH_C-400, respectively.

Ferrihydrite Transformation into Goethite. Goethite was synthesized from hydrothermal alteration of poorly crystalline ferrihydrite precursors described above, following a modified procedure from Schwertmann (2000).[41] The ferrihydrite slurries (FH_C-3000, FH_C-1000, FH_C-400, FH_S-3000, FH_S-1000, and FH_S-400) were adjusted to a pH of 10−11 using 1−5 mol/L KOH. The samples were placed in capped 30 mL Savillex PFA vials under atmospheric conditions and aged at 80 °C for 72 h in an oil bath to induce ferrihydrite transformation into goethite. The goethite samples will be referred to as G-FH_C-3000, G-FH_C-1000, G-FH_C-400, G-FH_S-3000, G-FH_S-1000, and G-FH_S-400. A schematic of the synthesis routes is presented in Figure 1.

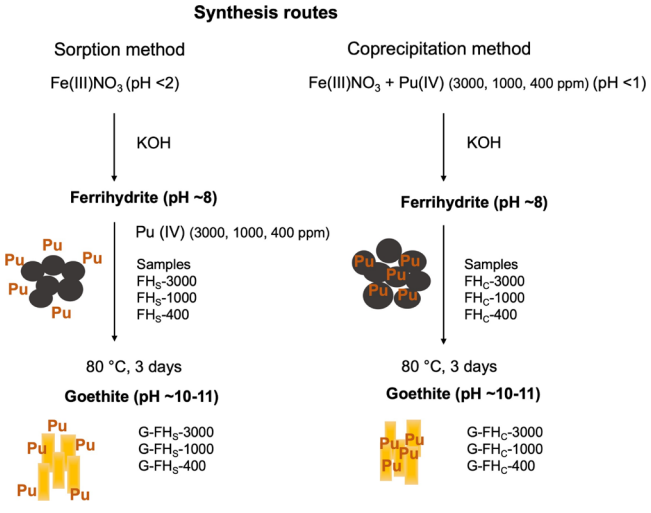


Figure 1. Schematics of synthesis routes of ferrihydrite and goethite solids synthesized via sorption and coprecipitation methods. Brown circles represent ferrihydrite precipitates and yellow rectangles represent goethite crystals.

After ferrihydrite and goethite synthesis, the supernatant was allowed to settle for 48 h, and after sedimentation an aliquot was centrifuged (4000 RCF, 50 min, ∼50 nm particle size cut off) and analyzed for Pu content via LSC. In preparation for the various microscopy and spectroscopy performed on the solid phase, the solids were rinsed and centrifuged (4000 RCF, 50 min, ∼50 nm particle size cut off) three times in Milli-Q water (18.2 MΩ·cm H_2O), to remove soluble salts. After each rinse, the supernatant was analyzed for Pu via LSC. Neither sedimentation nor centrifugation is expected to quantitatively remove Pu colloids from solution because an individual nanoparticle can be as small as 1.5−3 nm and nanoparticle aggregates may be tens of nm in size. To determine the nature of Pu in the supernatant, selected rinse solutions were filtered with 3 kDa ultrafiltration devices (Nanosep 3K Omega; approximate metric size discrimination: 1−2 nm; first rinse of G-FH_C-3000, and G-FH_S-3000). Results demonstrate that ∼80% of the total Pu in the supernatant is retained by the filter. This fraction of Pu could possibly include Pu associated with fine grained iron oxide minerals and/or Pu nanoparticle aggregates,[55] whereas the filtered fraction may include monomeric Pu(IV)[5] and possibly some individual Pu nanoparticles. The synthesis method described here contrasts with the work of Powell et al.[15] and Zavarin et al.[55] who added Pu directly to goethite in batch sorption experiments to examine adsorption and surface precipitation of Pu on the surface of goethite. By comparing these two synthesis strategies, we can gain insights into the mechanisms driving Pu associating with goethite.

Powder X-ray Diffraction. All Pu-doped goethite samples were prepared for powder X-ray diffraction (P-XRD) using a Bruker-D8 diffractometer from 5 to 70° (2θ). A domed zero background slide was loaded with 8−10 mg samples. The domed sample holder is necessary to avoid dispersion of radioactive materials; however, it introduces a high background especially at low angles. The introduction of this background makes it difficult to identify the presence of poorly crystalline amorphous material in the samples. For both ferrihydrite and goethite, Pu-free samples (FH-blank, G-blank) were prepared following the methodology described above, with which P-XRD measurements could be performed without the use of a domed sample holder.

Oxalate Extraction. To quantify ferrihydrite transformation into goethite, an oxalate extraction method was used.[41] For the oxalate extraction, 1 mL of pH 3 0.2 mol/L ammonium oxalate and 0.2 mol/L oxalic acid solution were added to a 2 mL (1 g/L) mineral slurry aliquot. The samples (G-FH_S-3000, G-FH_S-1000, G-FH_C-3000, and G-FH_C-1000) were then reacted in the absence of light on a shaker table for 2 h to dissolve any noncrystalline component. After 2 h, the samples were centrifuged (5 min, 4000 RFC) and the Fe concentration in the supernatant was determined via inductively coupled plasma mass spectrometry (Thermo Fisher Scientific ICAP-Q quadrupole ICP−MS). The oxalate extraction was also performed on one of the ferrihydrite samples (FH_S-3000).

Transmission Electron Microscopy. Mineral samples were suspended in ethanol (ferrihydrite) or Milli-Q water (18.2 MΩ·cm) (goethite), sonicated for 5 min and added dropwise onto a copper-supported lacy carbon grid. The samples were imaged using a Titan (FEI) microscope. Imaging was conducted at 300 kV using scanning electron and z-contrast modes. Energy-dispersive spectroscopy analyses were performed for selected areas and spots using a FEI SuperX G2 with quad silicon drift detectors. The structure of Pu colloids was investigated using high-resolution TEM (HR-TEM) and scanning TEM (STEM).

Pu Acid Extraction. Sequential acid extraction was performed to determine the leachability of Pu from the Pu-

https://dx.doi.org/10.1021/acsearthspacechem.0c00195
ACS Earth Space Chem. 2020, 4, 1993−2006

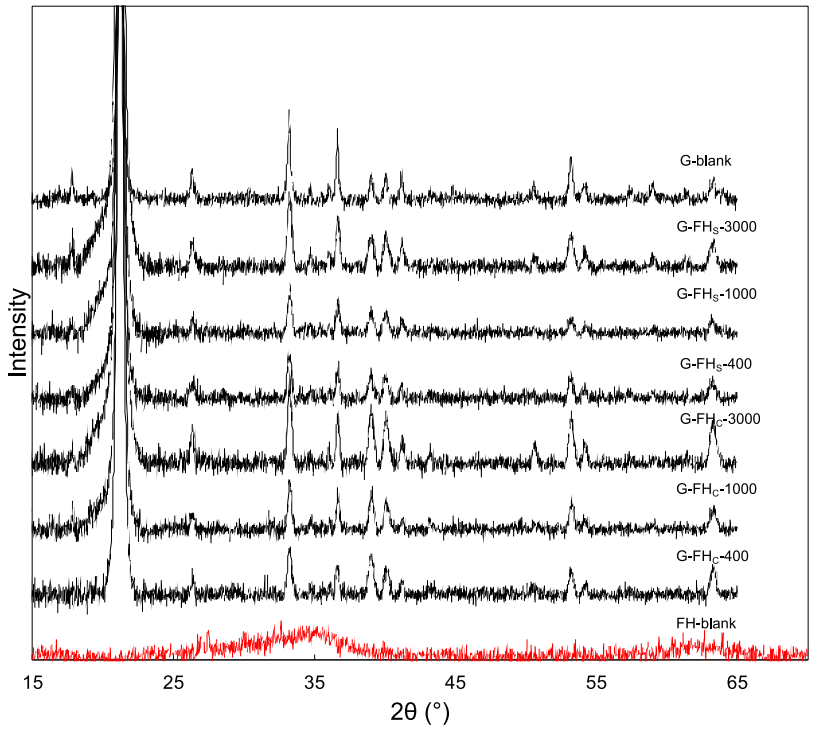


Figure 2. P-XRD pattern of Pu-free ferrihydrite and goethite (FH-blank, G-blank) and goethite samples G-FH_C-3000, G-FH_C-1000, G-FH_C-400, G-FH_S-3000, G-FH_S-1000, and G-FH_S-400.

doped goethite samples (G-FH_S-3000, G-FH_S-1000, G-FH_C-3000, and G-FH_C-1000). Mineral suspensions (0.33 g/100 mL) were equilibrated in increasingly higher molarity HNO_3 solutions (0.001−4 M) for 30 min. After 30 min extractions, the mineral-acid suspensions were centrifuged (10 min, 8500 RCF, size discrimination 100 nm) and the supernatant was analyzed to determine the Pu concentration via LSC. For G-FH_C-3000, G-FH_S-3000 an aliquot of the leached solution was filtered using a 3 kDa ultrafiltration device (Nanosep 3K Omega; approximate metric size discrimination: 1−2 nm). For both G-FH_C-3000 and G-FH_S-3000, the mineral suspensions in 4 M HNO_3 were reacted for an additional 20 h. Samples were then centrifuged (10 min, 8500 RCF) and the Pu concentrations in the supernatant were measured. A parallel experiment was performed on Pu-free goethite to determine the leachability of Fe. Fe concentrations in leached solutions were determined via inductively coupled plasma mass spectrometry (ICP−MS) (Thermo Fisher Scientific ICAP-Q quadrupole ICP−MS).

Extended X-ray Absorption Fine Structure Spectroscopy. Selected ferrihydrite and goethite mineral phases were isolated from the experiments via centrifugation (5 min, 4000 RCF), mixed with glycerol, and mounted into custom-made indium-sealed, triple-contained, aluminum sample holders. All EXAFS data were collected on beamline 11-2 at the Stanford Synchrotron Radiation Lightsource, Stanford CA. Pu L_{III}-edge (18057 eV) EXAFS data were collected in fluorescence mode using a 100 element Canberra Ge detector (corrected for dead time) with a Si(220) (ϕ = 0°) double monochromator detuned to 50% intensity. All samples were held in a LHe cryostat at 30 K throughout analysis. Data reduction and analysis were conducted using the RSXAP software suite[63−65] in conjunction with backscattering lineshapes and phases calculated using FEFF8.5L.[66] The EXAFS data were fitted in *R*-space. Error analysis was performed using a profiling method.[67] In all cases, the total number of fitting parameters was less than two-third of the total number of independent points.

■ RESULTS AND DISCUSSION

Ferrihydrite and Goethite Synthesis in the Presence of Pu(IV). After ferrihydrite and goethite were synthesized, the minerals were characterized by P-XRD, TEM, and oxalate extraction. P-XRD patterns of all goethite samples (G-FH_S-3000, G-FH_S-1000, G-FH_S-400, G-FH_C-3000, G-FH_C-1000, and G-FH_C-400) and of a Pu-free goethite sample were collected, and additional peaks beyond those characteristic of goethite were not identified (Figure 2). The P-XRD pattern of ferrihydrite was collected for FH-blank, a Pu free sample, and the broad peaks at 34° and 65° of 2θ are characteristic of two-line ferrihydrite.[41] TEM photomicrographs of the solid samples illustrate the crystal morphology of nanocrystalline FH_C-3000 and G-FH_C-3000 (Figure S1). The ferrihydrite nanoparticles are poorly crystalline and range in size between 3 and 5 nm, whereas the acicular goethite grains are crystalline and are 1−3 μm long and 10−100 nm wide. These crystal morphologies are consistent with ferrihydrite and goethite materials.[41] Oxalate extraction of G-FH_S-3000, G-FH_S-1000, G-FH_C-3000, and G-FH_C-1000 confirmed that >99% of ferrihydrite recrystallized to more ordered forms. As expected, the oxalate extraction of FH_S-3000 showed a total recovery of Fe (99.99%). The P-XRD, TEM analysis, and oxalate extraction results indicate that the addition of Pu does not affect the nature of the synthesized products (Figure 2).

The analysis of the supernatant from all ferrihydrite syntheses indicated that 99.9% of Pu had been removed from solution upon reaching the desired pH of ∼8. After ferrihydrite hydrothermal transformation into goethite, the concentration of Pu in the supernatant was monitored again

https://dx.doi.org/10.1021/acsearthspacechem.0c00195
ACS Earth Space Chem. 2020, 4, 1993−2006

and results show that for all samples <0.8% Pu was released in solution during rinsing (Figure S2). The results indicate that a strong association between Pu and the iron (oxy)hydroxide solids is preserved during ferrihydrite transformation into goethite, although a fraction of Pu may be mobilized during this process.

The HR-TEM imaging and elemental mapping of G-FH_S-3000 and G-FH_S-1000 revealed the presence Pu nanoparticles. As calculated from several TEM images, the size of the nanoparticles ranges from 3 to 5 nm, which is consistent with the 2.5−5 nm size range for PuO_2 reported in the literature.[5,16−18,55] Electron diffraction analysis of the HR-TEM data confirms that the observed nanoparticles have the expected face-centered cubic (fcc) PuO_2 structure with the *Fm*3*m* space group (d_1 (Å) 3.08(1) and d_2 (Å) 2.61(2))[15] (Figure 3). The observed PuO_2 structure is in contrast to the

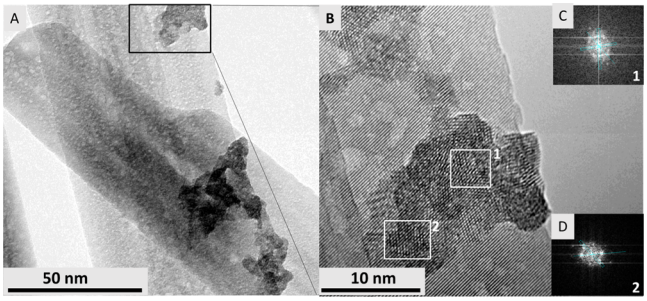


Figure 3. Pu nanoparticles on G-FH_S-3000. (A) Low-magnification TEM image of large tabular goethite and intrinsic Pu nanoparticles (black inlet). (B) HR-TEM image of Pu nanoparticles on the goethite surface from inlet in (A); (C,D) fast FT of HR-TEM areas 1 and 2 shown in panel (B) is consistent with the fcc, PuO_2 structure.

structure of Pu_4O_7 nanoparticles observed by Powell et al. (2011)[15] and Zavarin et al. (2014)[55] using TEM. The experiments of Zavarin et al. (2014)[55] examined the structure of Pu nanoparticles formed on the surface of goethite by the addition of a Pu source (either in the form of aqueous Pu(IV) or PuO_2 nanoparticles) in batch sorption experiments at 25 and 80 °C for over 100 days. Their results showed that once formed, the Pu_4O_7 nanoparticles were stable at 80 °C for over 100 days; however, when PuO_2 nanoparticles were added as a source of Pu, they did not alter to Pu_4O_7. The formation of distorted Pu_4O_7 nanoparticles with body-centered cubic structure is interpreted as a result of a strong binding of Pu with the goethite surface leading to epitaxial growth.[15,55] Given that we did not observe the formation of Pu_4O_7 nanoparticles via HR-TEM imaging, we must conclude that our synthesis pathways were not dominated by the epitaxial growth of Pu nanoparticles on the goethite surface. Instead, it is likely that PuO_2 observed here was formed during the ferrihydrite precipitation step, or in solution during ferrihydrite alteration to goethite, thus suggesting that the synthesis pathway affects the final state of Pu on the goethite surface. Nevertheless, the presence of Pu nanoparticulates in these samples is not unexpected. In the synthesis of the samples following the sorption method, a Pu stock is added to a ferrihydrite slurry solution at pH ∼ 8, and starting at circumneutral pH values and at the Pu concentrations used in these experiments (>10^{-8} M), Pu(IV) is generally expected to undergo rapid hydrolysis to form PuO_2 solids.[5,12]

HR-TEM imaging revealed the presence of PuO_2 precipitates (fcc, d_1 (Å) 3.08(2) and d_2 (Å) 2.61(2)) in the high Pu concentration G-FH_C-3000 (Figure 4); however, PuO_2 nanoparticles were not identified in G-FH_C-1000 and G-FH_C-400. Furthermore in G-FH_C-1000 and G-FH_C-400, the Pu concentration was too low to be detected using STEM−TEM indicating that Pu is either dispersed on the surface of goethite and/or incorporated into the solid phase.

Unfortunately, the ferrihydrite nanoparticles are 3−5 nm in size, which is similar to the expected PuO_2 nanoparticle size observed in the goethite samples (3−5 nm). This similarity in size between Pu nanoparticles and the ferrihydrite substrate creates difficulties in the identification and distinction of PuO_2 via TEM imaging (i.e., the needle in a haystack problem). For this reason, TEM was not sufficient to identify whether Pu nanoparticles were present in the ferrihydrite samples (FH_S-3000 and FH_C-3000), and we turn to EXAFS as a more definitive confirmation (below).

Reversibility of Pu Associated with Ferrihydrite and Goethite. In an effort to understand the reversibility of Pu associated with the goethite, acid leaching experiments were performed. In 4 h sequential leaching experiments (0.001−4 M), a total of 9.6 ± 0.2 and 3.42 ± 0.3% of Pu is leached from G-FH_S-3000 and G-FH_S-1000, respectively, whereas 4.03(12)% and 1.54(8)% of Pu is leached into solution from G-FH_C-3000 and G-FH_C-1000, respectively (Figure 5). The centrifuged supernatant likely includes particles <100 nm (Pu associated with goethite and/or Pu nanoparticle aggregates), and Pu aqueous species in the form of aqueous Pu(IV) at lower pH values.[5] Upon filtration with a 3 kDa filter of GFH_S-3000 and G-FH_C-3000, up to 70% of the total Pu is retained by the filter; however, as expected by thermodynamic and solubility considerations,[5] the amount of Pu filtered through a 3 kDa filter increases as the acidity of the leaching

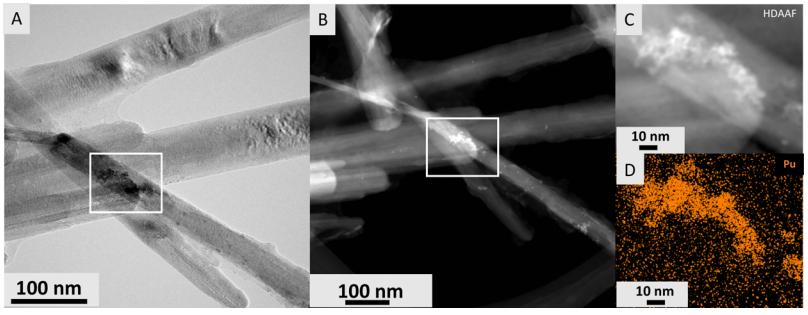


Figure 4. PuO_2 nanoparticles on G-FH_C-3000. (A) Low-magnification TEM and (B) STEM images of large tabular goethite and PuO_2 (white inlet). (C) STEM and (D) Pu elemental map of Pu nanoparticles.

https://dx.doi.org/10.1021/acsearthspacechem.0c00195
ACS Earth Space Chem. 2020, 4, 1993−2006

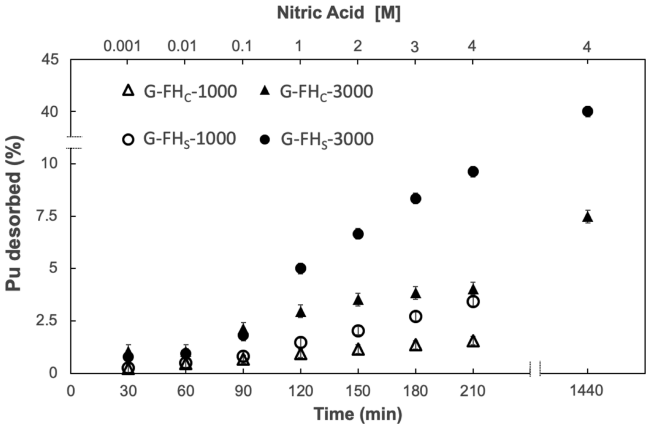


Figure 5. Leaching behavior of Pu in acidic solutions (0.001−4 M) for goethite synthesized following the sorption (G-FH_S-3000 and G-FH_S-1000) and coprecipitation (G-FH_C-3000 and G-FH_C-1000) method. Data shown with 2σ errors.

solution increases (Figure S3). After an additional 20 h of leaching in a 4 mol/L HNO_3 solution, a total of 40(1)% of Pu is leached from G-FH_S-3000, whereas only 7.5(5)% of total Pu is leached from G-FH_C-3000 (Figure 5). In the Pu-free goethite leaching test, <0.05 ± 0.003% Fe was dissolved after 24 h, indicating that goethite dissolution during the leaching process was minimal (Figure S4).

Overall, the majority of Pu remain associated with goethite, and in all experiments <40% of Pu is leached from goethite, regardless of the synthetic route. Differences in synthetic pathways, however, appear to have an impact on the nature of Pu association with the hydrothermally transformed product (goethite), as in just 4 h of sequential leaching (Figure 5) two to three times more Pu is leached from goethite recrystallized following the sorption process, compared to the coprecipitated samples. These results suggest that Pu associated with ferrihydrite/goethite through the sorption method may be more labile than Pu coprecipitated with ferrihydrite/goethite. Furthermore, the fact that a larger fraction of Pu is leachable in high Pu concentration compared to low Pu concentration samples suggests that the fraction of surface-associated Pu increases with concentration. This increase may indirectly suggest a limited capacity for Pu to be incorporated into the goethite phase (and not susceptible to leaching). Leaching experiments could not be performed on the ferrihydrite samples because of the enhanced dissolution of ferrihydrite in the chosen experimental conditions, nonetheless these results suggest that some properties of Pu association with the precursor mineral are retained through the transformation of ferrihydrite into goethite.

Structure of Pu Associated with Ferrihydrite and Goethite Using EXAFS. A representative set of ferrihydrite and goethite samples was analyzed using EXAFS spectroscopy in order to characterize the nature of Pu binding with these mineral phases. Three samples following the sorption method, FH_S-3000, G-FH_S-3000, and G-FH_S-1000, were analyzed in addition to four samples that were produced from the coprecipitated method, FH_C-3000, G-FH_C-3000, G-FH_C-1000, and G-FH_C-400. The background-subtracted Pu L_{III}-edge EXAFS spectra and the corresponding Fourier transforms (FT) for ferrihydrite and goethite systems are shown in Figures 6 and 7, and the fitting results for all datasets are detailed in Table 1. Corresponding X-ray absorption near edge spectra for these samples are shown in Figure S5 and the calculated edge inflection energies are tabulated in Table S1.

Ferrihydrite. The EXAFS spectrum of FH_S-3000 was successfully modeled with a single Pu−O shell consisting of 9(1) scatterers (i.e., coordination number) at 2.31(1) Å. Further two peaks were evident in the FT at r > 2.5 Å. Note that we refer to the x-axis of the FT as r, which differs from pair distances (R) because of the known shift effects.[66] The first of the two peaks was successfully modeled as 6(4) Pu−Fe scatterers at 3.39(1) Å with an elevated Debye Waller factor (σ^2; pair-distance distribution variance) of 0.021(4) $Å^2$, which implies a broad distribution of Pu−Fe distances. Alternatively, as σ^2 and coordination number are correlated in the EXAFS equation, it could be that the number of Pu−Fe scatterers is being overestimated. Normally, this correlation would be accounted for in the error estimates; however, in the case of non-Gaussian pair-distance distributions (e.g., a split-shell that is not resolved), the error estimates and best-fit parameters can be inaccurate. For example, Table S2 shows two alternative fitting models for this dataset. The first demonstrates that fixing the number of coordinating Fe atoms to three still produces a high-quality fit while reducing the σ^2 to a more reasonable (albeit still elevated) 0.015 $Å^2$. The second fit utilizes a Pu−Fe shell that was allowed to split into two. This model produced a fit with 1.9(5) and 1.0(5) Pu−Fe scatterers at 3.28(5) and 3.43(3) Å, respectively. Given these alternative fits, it seems likely the number of Pu−Fe scatterers is being significantly overestimated in our standard fit and the true value is more in line with a Pu−ferrihydrite sorption complex. The second peak was modeled with 3(1) Pu−Pu scatterers at 3.79(1) Å, consistent with expectations for PuO_2 (3.82 Å).[68] Given the identification of both Pu and Fe scatterers in the EXAFS, it is very likely that in FH_S-3000, Pu(IV) is present in two distinct coordination environments: PuO_2, and an additional adsorbed, poorly defined, inner-sphere complex on the ferrihydrite surface. Recent reports of various actinides (An = Th, U, Np, and Pu) adsorbed onto Fe containing minerals show An−Fe distances varying from 3.35 to 3.7 Å,[48,69−73] consistent with our modeled 3.39(1) Å Pu−Fe distance. Alternatively, these EXAFS data could be explained by a coordination environment containing an interaction between PuO_2 and the ferrihydrite surfaces that is a PuO_2 nanoparticle associated with the ferrihydrite where it can "see" surface Fe atoms. This could also explain some of the high Debye−Waller factors we observe. However, on balance, a dual coordination environment with PuO_2 and a Pu−ferrihydrite complex seems more likely, especially given the similarity in reported Pu−Fe distances. It is difficult to quantify the relative proportions of these two Pu species (inner-sphere and PuO_2) as EXAFS analysis only provides an average coordination environment around the Pu atom. However, we can use our knowledge of the PuO_2 structure to put a lower limit on the amount of PuO_2 in the sample. The structure of bulk PuO_2 consists of 12 Pu atoms at 3.82 Å,[68] which given our fitted coordination number of 3 Pu atoms would imply the minimum proportion of PuO_2 in this sample is ∼25%. However, the number of Pu atoms reduces as PuO_2 moves away from a bulk material into a nanoparticulate form because of the Pu atoms near the surface having fewer Pu neighbors (Figure S6).[70,74] This effect is well demonstrated for PuO_2 nanoparticles recently by Micheau et al., 2020,[18] which demonstrated that EXAFS can significantly underestimate the particle size when compared to

https://dx.doi.org/10.1021/acsearthspacechem.0c00195
ACS Earth Space Chem. 2020, 4, 1993−2006

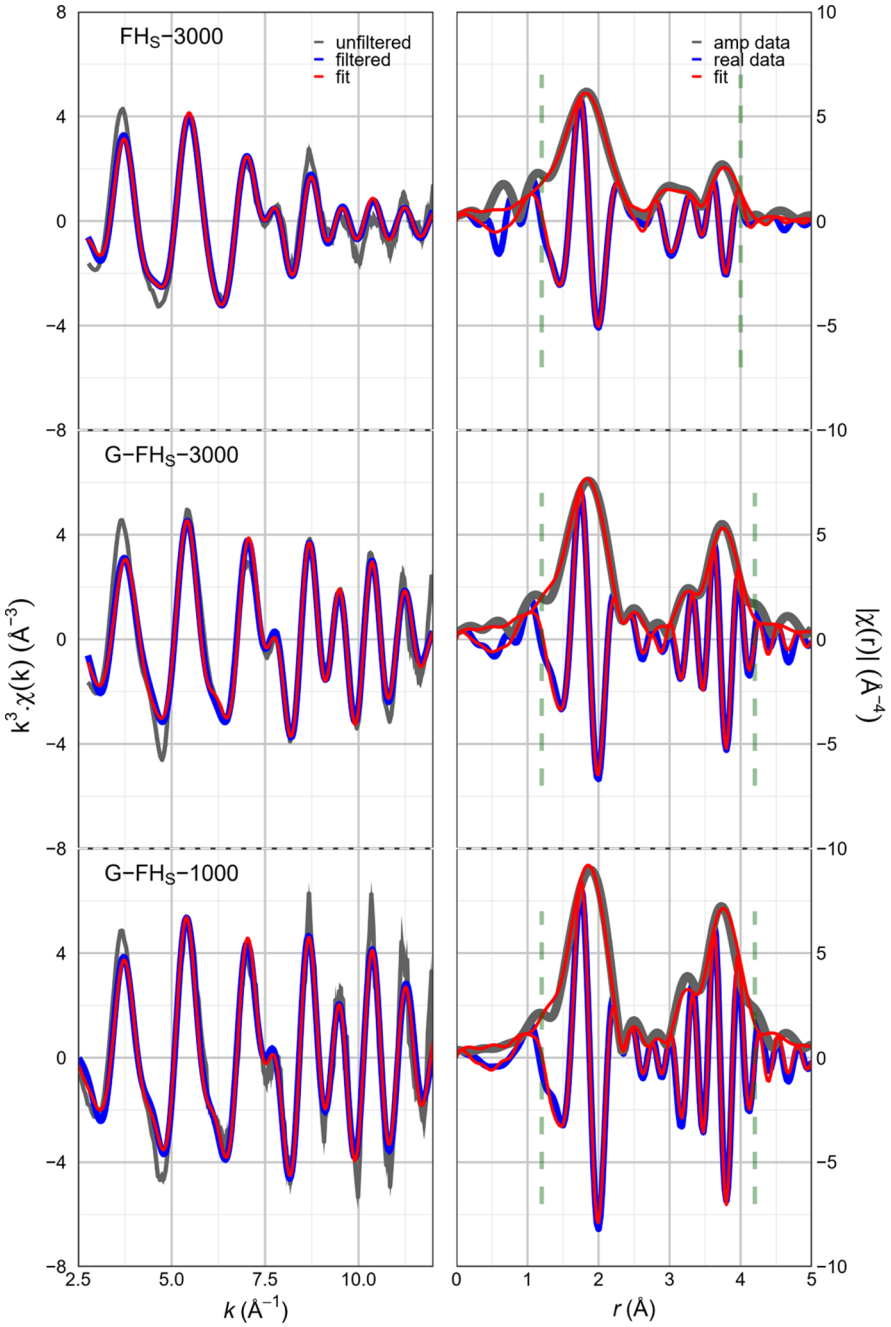


Figure 6. Pu L_{III}-edge EXAFS data and fit results for samples synthesized following the sorption method measured at 30 K. Left: EXAFS results in *k*-space. Right: FT of the *k*-space data and fit. Vertical dashed lines indicate the fit range. Data were transformed between 2.5 and 12 $Å^{-1}$ by using a Gaussian window with a width of 0.3 $Å^{-1}$. The raw unfiltered data error bars (encompassed by the solid gray shaded area around the data set) were estimated by the standard deviation of the mean between traces.

small angle X-ray scattering measurements. Therefore, because of these effects, this value only represents a lower limit on the proportion of PuO_2 in the sample. This also implies the maximum proportion of PuO_2 that is surface adsorbed is 75%. Overall, the EXAFS results indicate a significant degree of surface adsorption and PuO_2 precipitation.

The EXAFS spectrum of Pu associated with FH_C-3000 was successfully modeled with a split O environment, including 3.0(1) and 4.0(2) Pu−O scatterers at 2.24(1) and 2.41(1) Å, respectively. In contrast to FH_S-3000, only one additional peak was evident in the FT, which was successfully fit with a single Pu−Fe shell at 3.39(1) Å. Interestingly, this shell was fit with a high number (8 ± 1) of Pu−Fe scatterers albeit with a very high σ^2 of 0.026(3) $Å^2$. The high uncertainties associated with this fit make the exact nature of the Pu−ferrihydrite complex difficult to elucidate, but it could represent a replacement of the Fe^{3+} ion with a Pu^{4+} in the ferrihydrite solid. The large discrepancy in the size of Fe^{3+} and Pu^{4+} ions (0.645 and 0.96, respectively[75]) make this substitution unlikely without significant disruption to the local structure. However, our EXAFS data do indicate highly elevated σ^2 values suggesting a broad range of Pu−Fe pair distances, and lack long-range order that would be evidenced by multiple Pu−Fe shells. The local environment around Fe in the

https://dx.doi.org/10.1021/acsearthspacechem.0c00195
ACS Earth Space Chem. 2020, 4, 1993−2006

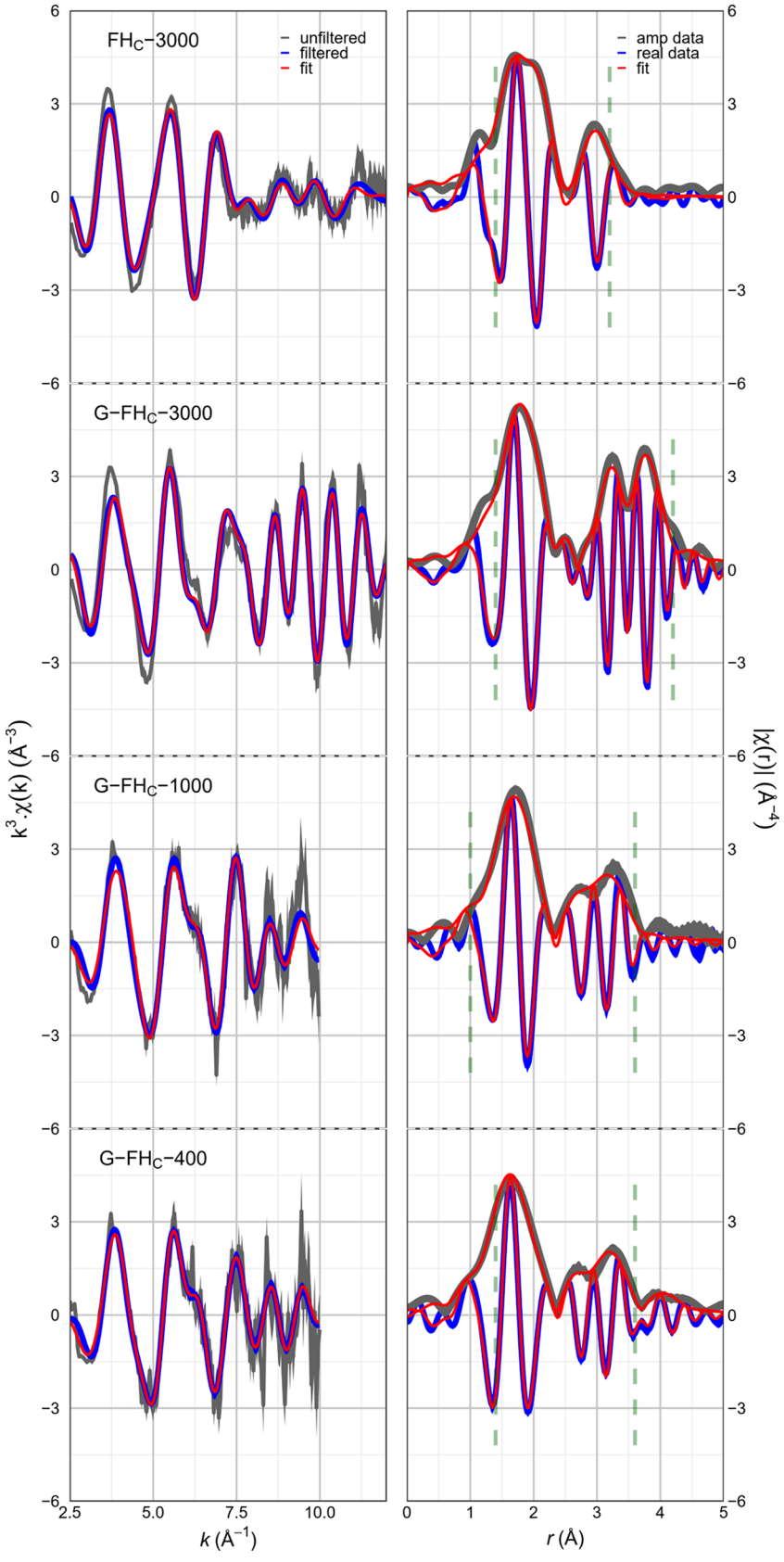


Figure 7. Pu L_{III}-edge EXAFS data and fit results for samples synthesized following the coprecipitation method measured at 30 K. Left: EXAFS results in *k*-space. Right: FT of the *k*-space data and fit. Data are transformed over the displayed range in *k*-space. Vertical dashed lines indicate the fit range. See Figure 6 for further details.

https://dx.doi.org/10.1021/acsearthspacechem.0c00195
ACS Earth Space Chem. 2020, 4, 1993−2006

Table 1. Summary of the EXAFS Fit Results

sample	shell	N	R (Å)	Σ^2 (Å^2)	ΔE_0 (eV)	R (%)
FH_S-3000	Pu−O	9(1)	2.31(1)	0.014(1)	−10.8(8)	8.0
	Pu−Fe	6(4)	3.39(1)	0.021(4)		
	Pu−Pu	3(1)	3.79(1)	0.008(1)		
FH_C-3000	Pu−O1	4.0(2)	2.41(1)	0.005(1)[a]	−11.0(4)	3.5
	Pu−O2	3.0(1)	2.24(1)	0.005(1)[a]		
	Pu−Fe	8(1)	3.39(1)	0.023(2)		
G-FH_S-3000	Pu−O	8(1)	2.32(1)	0.010(1)	−11.4(8)	10.2
	Pu−Pu	4(1)	3.80(1)	0.003(1)		
G-FH_S-1000	Pu−O	8(1)	2.32(1)	0.008(1)	−11.7(7)	9.9
	Pu−Pu	4(1)	3.81(1)	0.001(1)		
G-FH_C-3000	Pu−O	6(1)	2.28(1)	0.013(2)	−12.6(12)	8.7
	Pu−Fe	1(1)	3.56(1)	0.003(4)		
	Pu−Pu	2(1)	3.80(1)	0.001(1)		
G-FH_C-1000	Pu−O	5(1)	2.21(1)	0.013(2)	−10.0(16)	13.3
	Pu−Fe	6(1)	3.17(4)	0.01(1)[a]		
	Pu−Fe	10(8)	3.49(2)	0.01(1)[a]		
G-FH_C-400	Pu−O	6(1)	2.20(2)	0.016(2)	−7.6(21)	12.2
	Pu−Fe	5(3)	3.19(2)	0.015(6)[a]		
	Pu−Fe	8(4)	3.47(2)	0.015(6)[a]		

[a]Indicates a tied σ^2 parameter (i.e., shared in two shells). N represents the coordination number assuming an amplitude reduction factor of one; R denotes the interatomic distance; σ^2 represents the Debye Waller factor; ΔE_0 represents the energy shift from the calculated Fermi energy level.

ferrihydrite structure consists of Fe atoms at ∼3.04 and 3.44 Å, although because of the poorly crystalline nature of ferrihydrite, its structure has still not been fully resolved.[38,76] Although highly disordered, a Pu−Fe distance of 3.39(1) Å could correspond to corner sharing between metal polyhedra in the ferrihydrite structure.[76,77]

The σ^2 and coordination number parameters in the EXAFS equation are commonly correlated in the fit results;[78] therefore, the elevated σ^2 values fitted here suggest either a large amount of structural disorder (i.e., a broad distribution of Pu−Fe pair distances) or that the number of Pu−Fe scatterers is being overestimated. For example, constraining the number of Pu−Fe scatterers to four reduced σ^2 to 0.013(2) Å^2 while still maintaining a reasonable fit albeit with an increased fit residual factor (R %) (7.9 vs 3.5%); thus, it cannot be excluded that the EXAFS data may represent a surface complex with a lower number of Pu−Fe scatterers.[48,69−73] Interestingly, the EXAFS spectrum and resulting fit for FH_C-3000 bears a striking resemblance to what was collected in similar experiments by Smith et al.,[48] where ferrihydrite precipitation was induced from a Pu−HNO_3 solution at pH 9. PuO_2 formation was not observed and the data were modeled with 4 Fe scatterers at 3.38(2) Å and attributed to the formation of a polynuclear multidentate complex with the ferrihydrite surface. In contrast to FH_S-3000, no Pu−Pu scatterers could be identified in the FH_C-3000 EXAFS spectrum precluding the possibility of PuO_2 formation in this sample and demonstrating that Pu(IV) is associated with the ferrihydrite solid before PuO_2 precipitation could occur. The association of Pu with a Fe(III) precipitate in the materials formed during the coprecipitation method is possible as the coprecipitation synthesis starts from an aqueous solution at pH < 1 and according to thermodynamic considerations, under these solution conditions, Fe(III) hydrolysis precipitates may form in solution starting at pH 1−2 (Figure 1).[79,80]

Goethite. The EXAFS spectra of the goethite samples recrystallized from the hydrothermally altered Pu-sorbed ferrihydrite (G-FH_S-3000 and G-FH_S-1000) are similar and both spectra could be fit using a two-shell model. The first shell in both cases was successfully fit with 8(1) Pu−O scatterers at 2.32(1) Å and the second peak in the FT was fit with 4(1) Pu−Pu scatterers at 3.80(1) Å strongly supporting the formation of PuO_2 solids in these systems. However, the modeled Pu coordination numbers are low compared to expectations for PuO_2 and suggest either PuO_2 is present as very small nanoparticulate <1 nm (Figure S6) or that a second Pu species is present as an adsorbed or a coprecipitated inner sphere complex. We use a similar approach with this sample as we used with FH_S-3000 and attempt to put a lower limit on the quantity of PuO_2 present. If we assume Pu is present as bulk (as opposed to nanoparticulate or surface-adsorbed)-PuO_2 with a Pu−Pu coordination number of 12, the number of Pu−Pu scatterers in both samples being fitted as 4(1) would indicate a minimum of 33% Pu is present as PuO_2 in this system, not unlike the FH_S-3000 precursor.

In this case, if the TEM characterized particles are representative of the average, the remaining Pu would have to be present as a surface complex. Unfortunately, while it was possible to include Pu−Fe scatterers in the fit their presence was unable to pass an F-test[81] so we cannot conclusively demonstrate an inner-sphere surface complex, however, this does not exclude the possibility of a surface complex entirely. For example, Pu may be present as an inner sphere complex with a very broad range of Pu−Fe pair distances making it very difficult to discern using EXAFS analysis. Interestingly, the minimum proportion of PuO_2 in the sample remains the same, prior to and after ferrihydrite transformation into goethite. This, in turn, may indicate that the PuO_2 does not undergo any transformation during the alteration of ferrihydrite to goethite.

Overall, the EXAFS fits and TEM characterization support PuO_2 formation in G-FH_S-3000 and G-FH_S-1000. The EXAFS data also suggest that Pu in these samples may be present in a dual coordination environment with PuO_2 accounting for a minimum of 33% of Pu, and the remainder being present as

https://dx.doi.org/10.1021/acsearthspacechem.0c00195
ACS Earth Space Chem. 2020, 4, 1993−2006

the poorly defined surface complex because no Pu−Fe scatterers could be conclusively identified in this sample.[11,12] Though it is important to stress that the PuO_2 calculation represents a floor (i.e., a minimum) and the real value is likely to be much higher because of nanoparticle/surface effects. The high percentage of Pu detected in the acid extraction of G-FH_S-3000 and G-FH_S-1000 is consistent with the presence of Pu as a surface complex, where the leached fraction could represent any bound Pu being easily leached from the goethite surface. Collectively, these data demonstrate that in the ferrihydrite and goethite samples synthesized following the sorption method, a fraction of Pu will be found as intrinsic PuO_2 nanoparticles, and the PuO_2-like coordination environment is preserved during mineral phase transformation. The EXAFS data also demonstrate that Pu adsorbed to ferrihydrite may be remobilized, as evidenced by the changes in the coordination environment of the Pu-sorbed species from the ferrihydrite precursor (FH_S-3000) to the recrystallized products (G-FH_S-1000 and G-FH_S-3000) (Table 1).

The EXAFS spectrum of the Pu associated with G-FH_C-3000 was successfully modeled with 6(1) Pu−O scatterers at 2.28(1) Å and 1 (1) Pu−Fe scatterers at 3.56(1) with σ^2 values of 0.013(2) and 0.003(1) $Å^2$, respectively. Pu−Fe σ^2 is very low and probably represents an underestimation of the number of Pu−Fe scatterers because of the coupling between σ^2 and the coordination number in the EXAFS equation. Additionally, a peak at 3.7 Å was successfully modeled as 2(1) Pu−Pu scatterers at 3.80(1). The clear identification of Pu−Pu scatterers in the FT demonstrates the presence of PuO_2. Interestingly, no PuO_2 was observed in the ferrihydrite precursor (FH_C-3000) indicating that Pu(IV) was probably excluded from the ferrihydrite structure or surface in the ferrihydrite transformation reaction where it subsequently underwent precipitation as PuO_2. As with the other observations of Pu−Pu scatterers in other samples presented here, the low coordination numbers suggest PuO_2 accounts for only a fraction of all Pu in this sample. A pair of Pu−Pu scatterers would imply a minimum of 17% PuO_2 in this experiment. The presence of Pu−Fe peaks suggests that the non-PuO_2 fraction of Pu in this sample may be present as an inner sphere complex adsorbed on the surface of goethite. Importantly, the results suggest that high Pu concentrations associated with ferrihydrite may lead to the formation of PuO_2 during the transformation of ferrihydrite into goethite.

The G-FH_C-1000 and G-FH_C-400 samples displayed similar spectra with three easily identifiable peaks in the FT at $r \approx$ 1.5, 2.5, and 3.2 Å. The first peak at 1.5 Å was successfully fit with Pu−O shell 6(1) scatterers at 2.21(1) Å. Oxygen shells in both G-FH_C-1000 and G-FH_C-400 have σ^2 factors of 0.013(2) and 0.016(2) $Å^2$ implying a broad distribution of Pu−O pair distances. This reduction in oxygen atom coordination from eight in the other systems to six here is interesting as Fe^{3+} is coordinated by six oxygen atoms in the goethite structure. Additionally, the Pu−O bond distances of 2.21 Å are significantly shorter than would be expected for a Pu(IV) surface complex and is closer to the Fe−O bond distance in goethite at ∼2.1 Å.[82,83] This bond distance is significantly shorter than that of the G-FH_C-3000 sample, which was fitted with a Pu−O distance of 2.28 Å. This lengthening of the bond with concentration can probably be attributed to an averaging effect caused by the presence of two distinct coordination environments: one with a shorter Pu−O distance like we see here for G-FH_c-400 and G-FH_c-1000; and second more typical of a PuO_2 environment. The second and third features in the FT were too short to be associated with Pu−Pu scatterers; therefore, they were modeled as two Fe shells. These were fitted as 6(1) Pu−Fe scatterers at 3.17(4) Å and 10(8) Pu−Fe scatterers at 3.49(2) Å with an elevated σ^2 factor of 0.010(1) $Å^2$ for G-FH_C-1000. This result is similar to that of G-FH_C-400 where the second and third features in the FT were fit as 5(3) Pu−Fe scatterers at 3.19(1) Å and 8(4) Pu−Fe scatterers at 3.47(2) Å. The high number of Fe atoms and the large estimated errors associated with those parameters in G-FH_C-1000 and G-FH_C-400 make it difficult to draw any firm conclusions about the exact nature of the local structure in the Pu−goethite complex. However, collectively, these EXAFS data could indicate that some kind of incorporation into the goethite structure is occurring. First, there is a reduction in the number of Pu−O scatterers to ∼6 and concurrent contraction in the Pu−O bond length to just ∼2.2 Å, which seems more plausible for the Pu^{4+} ion in a G-like structure rather than a surface complex.

Furthermore, the local environment around Fe in the goethite structure consists of two, two, and four Fe neighbors at ∼3, ∼3.3, and ∼3.4 Å, respectively.[82,83] These distances are not unlike our fitted distances of 3.2 and 3.5 Å and given the large error bars associated with our fits, our data are compatible with those of Pu^{4+} incorporated into goethite. As was discussed previously, the difference in size between Fe^{3+} and Pu^{4+} makes direct and stable substitution into the goethite structure unlikely without significant disorder in the local and long-range structure. Interestingly, σ^2 in our fits suggests elevated levels of local structural disorder around the Pu atom. Other possible explanations for the local Pu structure observed are the formation of a surface complex on the goethite surface; however, the shortest modeled Pu−Fe distance at 3.19(2) Å is significantly shorter than the range of An−Fe distances previously reported (3.35−3.7 Å).[48,69−73] Finally, the EXAFS data are not inconsistent with the formation of a distinct poorly ordered Pu−Fe solid phase as has been hinted at in the forensics literature,[60] although the formation of a distinct Pu−Fe phase was not supported by TEM imaging. Overall, the TEM and EXAFS data demonstrate that PuO_2 exists at the highest concentration Pu coprecipitation samples (3000 ppm) but not the lower concentrations (1000 and 400 ppm). This suggests that during ferrihydrite phase transformation at higher Pu concentration (0.06 mmol/L Pu(IV) in solution, 3000 ppm Pu(IV) in the solid) part of the Pu associated with the ferrihydrite precursor FH_C-3000 will be remobilized and form PuO_2 nanoparticles. Furthermore, there is evidence that during ferrihydrite transformation at a high Pu concentration, a fraction of Pu remains strongly bound to the goethite surface (Table 1). No PuO_2 was observed in the ferrihydrite precursor (FH_C-3000) or in the lower concentration goethite samples (G-FH_C-1000 and G-FH_C-400). The presence of two distinct Pu−Fe shells in G-FH_C-1000 and G-FH_C-400 (at 3.20 Å and 3.49 Å) compared to the ferrihydrite precursor FH_C-3000 (one shell at 3.41 Å) suggests that the Pu binding site changes significantly during iron oxide transformation. Even though Pu coordination changes during phase transformation, these experimental conditions do not favor PuO_2 precipitation. It is difficult to determine the exact nature of Pu in solids prepared following the coprecipitation process; however, the data clearly show that Pu is strongly bound to

https://dx.doi.org/10.1021/acsearthspacechem.0c00195
ACS Earth Space Chem. 2020, 4, 1993−2006

the minerals either by the formation of a strong inner sphere complex, or via an incorporation process.

CONCLUSIONS

In this study, we investigated the fate of Pu during iron oxide crystallization and phase transformation via TEM imaging, EXAFS, and chemical analysis. We show that variations in synthetic routes impact the nature of Pu associated with both the ferrihydrite precursor and the ferrihydrite phase-transformed product (goethite). When a Pu containing solution is added to a ferrihydrite mineral (sorption route), a fraction of the Pu precipitates as PuO_2 nanoparticles and the remaining Pu fraction forms a complex on the mineral surface. After hydrothermal alteration to goethite, the PuO_2-like nanoparticle is preserved as demonstrated by TEM imaging, and a fraction of Pu is still present as a surface-adsorbed species on the goethite mineral surface. There is evidence that this adsorbed species is more weakly bound to goethite than to ferrihydrite, as demonstrated by a lack of Pu−Fe scatterers in the goethite samples compared to the ferrihydrite precursor. This observation suggests that Pu adsorbed to ferrihydrite may be mobilized during the phase transformation. The analysis of the supernatant after hydrothermal alteration of ferrihydrite to goethite showed a small increase in the Pu concentration confirming that some Pu remobilization occurs during ferrihydrite transformation into goethite.

When ferrihydrite is precipitated directly from a solution containing Fe and Pu (coprecipitation route), no PuO_2 is observed. Although it is difficult to identify the exact nature of Pu in the sample because of a high degree of disorder, there is evidence that Pu is strongly bound to the ferrihydrite solids through a combination of adsorption and/or coprecipitation as evidenced by the high number of Pu−Fe scatterers. In these samples, a fraction of Pu could coprecipitate with ferrihydrite and/or form an inner sphere complex with multiple Fe sites. The EXAFS data show that the Pu binding site changes significantly during ferrihydrite transformation into goethite, indicating that Pu is mobilized during hydrothermal alteration; however, only a small fraction of Pu in the highest Pu concentration samples (G-FH_C-3000) is remobilized to form PuO_2. In all goethite samples, Pu is strongly sorbed (either coprecipitated and/or adsorbed as the inner sphere complex) to the goethite as evidenced by the presence of Pu−Fe scatterers. The acid leaching results support this conclusion by showing that less Pu is accessible to leaching in goethite formed via the coprecipitation process, compared to the goethite formed via the sorption process. These observations confirm that the nature of Pu associated with the mineral will affect the leachability of Pu from the solids and suggests that a fraction of the Pu may be incorporated into the goethite structure either in a distorted Fe crystallographic position or may coprecipitate as a separate phase.

Implications for the Natural and Engineered Environment. Our results show that variations in the synthetic routes (sorption vs coprecipitation) of ferrihydrite at pH ∼ 8 impact the nature of Pu associated with the mineral. The major difference between the two synthetic processes is the timing of Pu addition to the ferrihydrite precipitate and we expect both processes to be of environmental relevance. For example, the sorption method, where Pu is added at pH ∼ 8 to an already formed ferrihydrite, simulates a simple scenario where Pu becomes associated with a pre-existing mineral substrate. In the coprecipitation method, a Pu−ferrihydrite precipitate is formed from neutralizing the pH of an acidic solution containing dissolved Pu and Fe. This synthetic method likely simulates a scenario where an acidic plume is neutralized for remediation purposes or where changes in geochemical conditions occur in contaminated streams or ponds (e.g., the Mayak site[84]). Secondary iron (oxy)-hydroxides with associated Pu and other radionuclides have been identified in surface-contaminated waters in a pH range of 5.9−8.2[59,61,85] and although the mechanisms of formation of these radioactive particles is still unclear, both sorption and secondary mineral formation processes are likely involved.[59,61,85]

Our results also show that differences that exist in the Pu association with the precursor material are retained through transformation into goethite. The hydrothermal alteration to goethite, however, was conducted in the alkaline to hyperalkaline pH range (∼10−11). Many underground repository concepts utilize cementitious materials in the design as part of the engineered barrier system or as structural materials.[86] The pH during leaching of these materials upon resaturation will buffer to hyperalkaline conditions (pH 10.5−13.1), creating a plume of alkaline fluid in the host rock and/or local environment.[86] Furthermore, hyperalkaline conditions can prevail in many contaminated land scenarios, for example, where cementitious building materials contact subsurface sediments[87,88] and at the underground waste storage tanks at the Hanford Site in Washington State, USA.[89]

Overall, the results presented in this study provide valuable new insights into Pu(IV)−iron (oxy)hydroxide interactions in the natural and engineered environment and highlight the importance of understanding the fate of radionuclides during mineral phase transformation processes.

ASSOCIATED CONTENT

Supporting Information

The Supporting Information is available free of charge at https://pubs.acs.org/doi/10.1021/acsearthspacechem.0c00195.

TEM and STEM images of FH_C-3000 and of G-FH_C-3000; concentration of Pu measured via LSC for the supernatant, first and second rinse; leaching behavior of Pu (%) in acidic solution (0.001-4M) for G-FH_S-3000 (black: centrifuged supernatant and gray: filtered with 3 kDa ultrafiltration device) and G-FH_C-3000 (dark blue: centrifuged supernatant and light blue: filtered with 3 kDa ultrafiltration device); leaching behavior of Fe in acidic solution (0.001−4 M) for Pu-free G; Pu L_{III}-edge XANES spectra collected from Pu−ferrihydrite/Pu-goethite samples in this study; average Pu coordination number with respect to particle size in PuO_2 solids as calculated using Calvin analysis;[90] edge inflection point (edge energy, E_0) of Pu−ferrihydrite/Pu−goethite samples in this study; and alternative EXAFS fits for FH-S-3000. LLNL-JRNL-812443 (PDF)

AUTHOR INFORMATION

Corresponding Author

Enrica Balboni − *Glenn T. Seaborg Institute, Physical & Life Sciences Directorate, Lawrence Livermore National Laboratory, Livermore, California 94550, United States;* orcid.org/0000-0001-5988-3563; Phone: 925-422-4833; Email: balboni1@llnl.gov

https://dx.doi.org/10.1021/acsearthspacechem.0c00195
ACS Earth Space Chem. 2020, 4, 1993−2006

Authors

Kurt F. Smith − *Chemical Sciences Division, Lawrence Berkeley National Laboratory, Berkeley, California 94720, United States*

Liane M. Moreau − *Chemical Sciences Division, Lawrence Berkeley National Laboratory, Berkeley, California 94720, United States*

Tian T. Li − *Material Science Division, Physical & Life Sciences Directorate, Lawrence Livermore National Laboratory, Livermore, California 94550, United States*

Melody Maloubier − *Department of Environmental Engineering & Earth Sciences, Clemson University, Clemson, South Carolina 29634, United States*

Corwin H. Booth − *Chemical Sciences Division, Lawrence Berkeley National Laboratory, Berkeley, California 94720, United States*

Annie B. Kersting − *Glenn T. Seaborg Institute, Physical & Life Sciences Directorate, Lawrence Livermore National Laboratory, Livermore, California 94550, United States*

Mavrik Zavarin − *Glenn T. Seaborg Institute, Physical & Life Sciences Directorate, Lawrence Livermore National Laboratory, Livermore, California 94550, United States;* orcid.org/0000-0002-2426-6706

Complete contact information is available at: https://pubs.acs.org/10.1021/acsearthspacechem.0c00195

Notes

The authors declare no competing financial interest.

■ ACKNOWLEDGMENTS

Work at Lawrence Livermore National Laboratory was performed with funding from the Spent Fuel and Waste Science and Technology campaign of the U.S. Department of Energy's Nuclear Energy Program and the Department of Energy, Office of Science, Biological and Environmental Research, Subsurface Biogeochemical Research program (SCW1053) and performed under the auspices of the U.S. Department of Energy by Lawrence Livermore National Laboratory under Contract DE-AC52-07NA27344. Work at Lawrence Berkeley National Laboratory was supported by the Department of Energy, Office of Science, Biological and Environmental Research, Subsurface Biogeochemical Research program (SCW1053) under a subcontract with Lawrence Livermore National Laboratory. EXAFS measurements were performed at beamlines 11-2 at the Stanford Synchrotron Radiation Lightsource, which is supported by the U.S. Department of Energy, Office of Science, Office of Basic Energy Sciences under contract no. DE-AC02-76SF00515. LLNL-JRNL-812443.

■ REFERENCES

(1) Choppin, G. R. Redox speciation of plutonium in natural waters. *J. Radioanal Nucl. Chem.* **1991**, *147*, 109−116.

(2) Sanchez, A. L.; Murray, J. W.; Sibley, T. H. The adsorption of plutonium IV and V on goethite. *Geochim. Cosmochim. Acta* **1985**, *49*, 2297−2307.

(3) Begg, J. D.; Edelman, C.; Zavarin, M.; Kersting, A. B. Sorption kinetics of plutonium (V)/(VI) to three montmorillonite clays. *Appl. Geochem.* **2018**, *96*, 131−137.

(4) Efurd, D. W.; Runde, W.; Banar, J. C.; Janecky, D. R.; Kaszuba, J. P.; Palmer, P. D.; Roensch, F. R.; Tait, C. D. Neptunium and Plutonium Solubilities in a Yucca Mountain Groundwater. *Environ. Sci. Technol.* **1998**, *32*, 3893−3900.

(5) Neck, V.; Altmaier, M.; Seibert, A.; Yun, J. I.; Marquardt, C. M.; Fanghaenel, T. Solubility and redox reactions of Pu(IV) hydrous oxide: Evidence for the formation of PuO2+x(s, hyd). *Radiochim. Acta* **2007**, *95*, 193−207.

(6) Zhao, P.; Zavarin, M.; Leif, R. N.; Powell, B. A.; Singleton, M. J.; Lindvall, R. E.; Kersting, A. B. Mobilization of actinides by dissolved organic compounds at the Nevada Test Site. *Appl. Geochem.* **2011**, *26*, 308−318.

(7) Icopini, G. A.; Lack, J. G.; Hersman, L. E.; Neu, M. P.; Boukhalfa, H. Plutonium(V/VI) Reduction by the Metal-Reducing Bacteria Geobacter metallireducens GS-15 and Shewanella oneidensis MR-1. *Appl. Environ. Microbiol.* **2009**, *75*, 3641−3647.

(8) Powell, B. A.; Fjeld, R. A.; Kaplan, D. I.; Coates, J. T.; Serkiz, S. M. $Pu(V)O_2^+$ adsorption and reduction by synthetic magnetite (Fe_3O_4). *Environ. Sci. Technol.* **2004**, *38*, 6016−6024.

(9) Zavarin, M.; Powell, B. A.; Bourbin, M.; Zhao, P.; Kersting, A. B. Np(V) and Pu(V) Ion Exchange and Surface-Mediated Reduction Mechanisms on Montmorillonite. *Environ. Sci. Technol.* **2012**, *46*, 2692−2698.

(10) Begg, J. D.; Zavarin, M.; Kersting, A. B. Desorption of plutonium from montmorillonite: An experimental and modeling study. *Geochem. Cosmochim. Acta* **2017**, *197*, 278−293.

(11) Choppin, G. R. Solution chemistry of the actinides. *Radiochim. Acta* **1983**, *32*, 43−53.

(12) Clark, D. L.; Hobart, D. E.; Neu, M. P. Actinide Carbonate Complexes and their Importance in Actinide Environmental Chemistry. *Chem. Rev.* **1995**, *95*, 25−48.

(13) Maher, K.; Bargar, J. R.; Brown, G. E., Jr. Environmental Speciation of Actinides. *Inorg. Chem.* **2013**, *52*, 3510−3532.

(14) Begg, J. D.; Zavarin, M.; Tumey, S. J.; Kersting, A. B. Plutonium sorption and desorption behavior on bentonite. *J. Environ. Radioact.* **2015**, *141*, 106−114.

(15) Powell, B. A.; Dai, Z.; Zavarin, M.; Zhao, P.; Kersting, A. B. Stabilization of Plutonium Nano-Colloids by Epitaxial Distortion on Mineral Surfaces. *Environ. Sci. Technol.* **2011**, *45*, 2698−2703.

(16) Dalodière, E.; Virot, M.; Morosini, V.; Chave, T.; Dumas, T.; Hennig, C.; Wiss, T.; Blanco, O. D.; Shuh, D. K.; Tyliszcak, T.; Venault, L.; Moisy, P.; Nikitenko, S. I. Insights into the sonochemical synthesis and properties of salt-free intrinsic plutonium colloids. *Sci. Rep.* **2017**, *7*, 43514.

(17) Gerber, E.; Romanchuk, A. Y.; Pidchenko, I.; Amidani, L.; Rossberg, A.; Hennig, C.; Vaughan, G. B. M.; Trigub, A.; Egorova, T.; Bauters, S.; Plakhova, T.; Hunault, M. O. J. Y.; Weiss, S.; Butorin, S. M.; Scheinost, A. C.; Kalmykov, S. N.; Kvashnina, K. O. The missing pieces of the PuO2 nanoparticle puzzle. *Nanoscale* **2020**, *12*, 18039.

(18) Micheau, C.; Virot, M.; Dourdain, S.; Dumas, T.; Menut, D.; Solari, P. L.; Venault, L.; Diat, O.; Moisy, P.; Nikitenko, S. I. Relevance of formation conditions to the size, morphology and local structure of intrinsic plutonium colloids. *Environ. Sci.: Nano* **2020**, *7*, 2252.

(19) Moreau, L. M.; Herve, A.; Straub, M. D.; Russo, D. R.; Abergel, R. J.; Alayoglu, S.; Arnold, J.; Braun, A.; Deblonde, G. J. P.; Liu, Y.; Lohrey, T. D.; Olive, D. T.; Qiao, Y.; Rees, J. A.; Shuh, D. K.; Teat, S. J.; Booth, C. H.; Minasian, S. G. Structural properties of ultra-small thorium and uranium dioxide nanoparticles embedded in a covalent organic framework. *Chem. Sci.* **2020**, *11*, 4648−4668.

(20) Begg, J. D.; Zavarin, M.; Zhao, P.; Tumey, S. J.; Powell, B.; Kersting, A. B. Pu(V) and Pu(IV) Sorption to Montmorillonite. *Environ. Sci. Technol.* **2013**, *47*, 5146−5153.

(21) Hixon, A. E.; Hu, Y.-J.; Kaplan, D.; Kukkadapu, R. K.; Nitsche, H.; Qafoku, O.; Powell, B. A. Influence of iron redox transformations on plutonium sorption to sediments. *Radiochim. Acta* **2010**, *98*, 685−692.

(22) Kirsch, R.; Fellhauer, D.; Altmaier, M.; Neck, V.; Rossberg, A.; Fanghänel, T.; Charlet, L.; Scheinost, A. C. Oxidation state and local structure of plutonium reacted with magnetite, mackinawite, and chukanovite. *Environ. Sci. Technol.* **2011**, *45*, 7267−7274.

(23) Shaughnessy, D. A.; Nitsche, H.; Booth, C. H.; Shuh, D. K.; Waychunas, G. A.; Wilson, R. E.; Gill, H.; Cantrell, K. J.; Serne, R. J. Molecular interfacial reactions between Pu(VI) and manganese oxide

minerals manganite and hausmannite. *Environ. Sci. Technol.* **2003**, *37*, 3367−3374.
(24) Zhao, P.; Begg, J. D.; Zavarin, M.; Tumey, S. J.; Williams, R.; Dai, Z. R.; Kips, R.; Kersting, A. B. Plutonium(IV) and (V) Sorption to Goethite at Sub-Femtomolar to Micromolar Concentrations: Redox Transformations and Surface Precipitation. *Environ. Sci. Technol.* **2016**, *50*, 6948−6956.
(25) Romanchuk, A. Y.; Kalmykov, S. N.; Aliev, R. A. Plutonium sorption onto hematite colloids at femto- and nanomolar concentrations. *Radiochim. Acta* **2011**, *99*, 137−144.
(26) Marshall, T. A.; Morris, K.; Law, G. T. W.; Livens, F. R.; Mosselmans, J. F. W.; Bots, P.; Shaw, S. Incorporation of Uranium into Hematite during Crystallization from Ferrihydrite. *Environ. Sci. Technol.* **2014**, *48*, 3724−3731.
(27) Ferris, F. G.; Hallberg, R. O.; Lyvén, B.; Pedersen, K. Retention of strontium, cesium, lead and uranium by bacterial iron oxides from a subterranean environment. *Appl. Geochem.* **2000**, *15*, 1035−1042.
(28) Alberts, J. J.; Halverson, J. E.; Orlandini, K. A. The Distribution of Plutonium, Americium and Curium Isotopes in Pond and Stream Sediments of the Savannah River Plant, South-Carolina, USA. *J. Environ. Radioact.* **1986**, *3*, 249−271.
(29) Pinder, J. E.; Alberts, J. J.; Bowling, J. W.; Nelson, D. M.; Orlandini, K. A. The annual cycle of plutonium in the water column of a warm, monomictic reservoir. *J. Environ. Radioact.* **1992**, *17*, 59−81.
(30) Whicker, F. W.; Pinder, J. E.; Bowling, J. W.; Alberts, J. J.; Brisbin, I. L. Distribution of long-lived radionuclides in an abandoned reactor cooling reservoir. *Ecol. Monogr.* **1990**, *60*, 471−496.
(31) Benner, S. G.; Hansel, C. M.; Wielinga, B. W.; Barber, T. M.; Fendorf, S. Reductive dissolution and biomineralization of iron hydroxide under dynamic flow conditions. *Environ. Sci. Technol.* **2002**, *36*, 1705−1711.
(32) Luther, G. W.; Kostka, J. E.; Church, T. M.; Sulzberger, B.; Stumm, W. Seasonal Iron Cycling in the Salt-Marsh Sedimentary Environment - the Importance of Ligand Complexes with Fe(II) and Fe(III) in the Dissolution of Fe(III) Minerals and Pyrite, Respectively. *Mar. Chem.* **1992**, *40*, 81−103.
(33) King, F. 13—Nuclear waste canister materials: Corrosion behavior and long-term performance in geological repository systems. In *Geological Repository Systems for Safe Disposal of Spent Nuclear Fuels and Radioactive Waste*, 2nd ed; Apted, M. J., Ahn, J., Eds.; Woodhead Publishing, 2017; pp 365−408.
(34) Féron, D.; Crusset, D.; Gras, J.-M. Corrosion issues in nuclear waste disposal. *J. Nucl. Mater.* **2008**, *379*, 16−23.
(35) Musić, S.; Gotic, M.; Popovic, S. X-Ray-Diffraction and Fourier-Transform Infrared-Analysis of the Rust Formed by Corrosion of Steel in Aqueous-Solutions. *J. Mater. Sci.* **1993**, *28*, 5744−5752.
(36) El Hajj, H.; Abdelouas, A.; El Mendili, Y.; Karakurt, G.; Grambow, B.; Martin, C. Corrosion of carbon steel under sequential aerobic-anaerobic environmental conditions. *Corros. Sci.* **2013**, *76*, 432−440.
(37) Wersin, P.; Jenni, A.; Mäder, U. K. Interaction of Corroding Iron with Bentonite in the Abm1 Experiment at Aspo, Sweden: A Microscopic Approach. *Clays Clay Miner.* **2015**, *63*, 51−68.
(38) Michel, F. M.; Ehm, L.; Antao, S. M.; Lee, P. L.; Chupas, P. J.; Liu, G.; Strongin, D. R.; Schoonen, M. A. A.; Phillips, B. L.; Parise, J. B. The Structure of Ferrihydrite, a Nanocrystalline Material. *Science* **2007**, *316*, 1726−1729.
(39) Fischer, W. R.; Schwertmann, U. Formation of hematite from amorphous iron(III)hydroxide. *Clays Clay Miner.* **1975**, *23*, 33−37.
(40) Combes, J. M.; Manceau, A.; Calas, G. Formation Of Ferric Oxides From Aqueous-Solutions - A Polyhedral Approach By X-Ray Absorption-Spectroscopy. *Geochem. Cosmochim. Acta* **1990**, *54*, 1083−1091.
(41) Schwertmann, U.; Cornell, R. M. Iron oxides in the laboratory. *Iron Oxides in the Laboratory*; Wiley-VCH Verlag GmbH, 2000; pp i−xviii.
(42) Das, S.; Hendry, M. J.; Essilfie-Dughan, J. Transformation of Two-Line Ferrihydrite to Goethite and Hematite as a Function of pH and Temperature. *Environ. Sci. Technol.* **2011**, *45*, 268−275.
(43) Shaw, S.; Pepper, S. E.; Bryan, N. D.; Livens, F. R. The kinetics and mechanisms of goethite and hematite crystallization under alkaline conditions, and in the presence of phosphate. *Am. Mineral.* **2005**, *90*, 1852−1860.
(44) Ray, J. R.; Wan, W.; Gilbert, B.; Jun, Y.-S. Effects of Formation Conditions on the Physicochemical Properties, Aggregation, and Phase Transformation of Iron Oxide Nanoparticles. *Langmuir* **2013**, *29*, 1069−1076.
(45) Yang, R.; Tao, J.; Huang, Q.; Tie, B.; Lei, M.; Yang, Y.; Du, H. Co-adsorption of Cd(II) and Sb(III) by ferrihydrite: a combined XPS and ITC study. *J. Soils Sediments* **2019**, *19*, 1319−1327.
(46) Dyer, J. A.; Trivedi, P.; Scrivner, N. C.; Sparks, D. L. Lead Sorption onto Ferrihydrite. 2. Surface Complexation Modeling. *Environ. Sci. Technol.* **2003**, *37*, 915−922.
(47) Jain, A.; Loeppert, R. H. Effect of Competing Anions on the Adsorption of Arsenate and Arsenite by Ferrihydrite. *J. Environ. Qual.* **2000**, *29*, 1422−1430.
(48) Smith, K. F.; Morris, K.; Law, G. T. W.; Winstanley, E. H.; Livens, F. R.; Weatherill, J. S.; Abrahamsen-Mills, L. G.; Bryan, N. D.; Mosselmans, J. F. W.; Cibin, G.; Parry, S.; Blackham, R.; Law, K. A.; Shaw, S. Plutonium(IV) Sorption during Ferrihydrite Nanoparticle Formation. *ACS Earth Space Chem.* **2019**, *11*, 2437.
(49) Bots, P.; Shaw, S.; Law, G. T. W.; Marshall, T. A.; Mosselmans, J. F. W.; Morris, K. Controls on the Fate and Speciation of Np(V) During Iron (Oxyhydr)oxide Crystallization. *Environ. Sci. Technol.* **2016**, *50*, 3382−3390.
(50) Um, W.; Serne, R. J.; Brown, C. F.; Rod, K. A. Uranium(VI) sorption on iron oxides in Hanford Site sediment: Application of a surface complexation model. *Appl. Geochem.* **2008**, *23*, 2649−2657.
(51) Romanchuk, A. Y.; Gusev, I. V.; Vlasova, I. E.; Petrov, V. G.; Kuzmenkova, N. V.; Egorova, B. V.; Zakharova, E. V.; Volkova, A. G.; Kalmykov, S. N. Interaction of Plutonium with Iron- and Chromium-Containing Precipitates under the Conditions of Reservoir Bed for Liquid Radioactive Waste. *Radiochemistry* **2016**, *58*, 662−667.
(52) Sylvester, P.; Milner, T.; Jensen, J. Radioactive liquid waste treatment at Fukushima Daiichi. *J. Chem. Technol. Biotechnol.* **2013**, *88*, 1592−1596.
(53) Winstanley, E. H.; Morris, K.; Abrahamsen-Mills, L. G.; Blackham, R.; Shaw, S. U(VI) sorption during ferrihydrite formation: Underpinning radioactive effluent treatment. *J. Hazard. Mater.* **2019**, *366*, 98−104.
(54) McBriarty, M. E.; Soltis, J. A.; Kerisit, S.; Qafoku, O.; Bowden, M. E.; Bylaska, E. J.; De Yoreo, J. J.; Ilton, E. S. Trace Uranium Partitioning in a Multiphase Nano-FeOOH System. *Environ. Sci. Technol.* **2017**, *51*, 4970−4977.
(55) Zavarin, M.; Zhao, P.; Dai, Z.; Kersting Annie, B. Plutonium sorption and precipitation in the presence of goethite at 25 and 80 ○C. *Radiochim. Acta* **2014**, *102*, 983.
(56) Felmy, A. R.; Moore, D. A.; Qafoku, O.; Buck, E.; Conradson, S. D.; Ilton, E. S. Heterogeneous reduction of (PuO2)-Pu-239 by aqueous Fe(II) in the presence of hematite. *Radiochim. Acta* **2013**, *101*, 701−710.
(57) Dumas, T.; Fellhauer, D.; Schild, D.; Gaona, X.; Altmaier, M.; Scheinost, A. C. Plutonium Retention Mechanisms by Magnetite under Anoxic Conditions: Entrapment versus Sorption. *ACS Earth Space Chem.* **2019**, *3*, 2197−2206.
(58) Joseph, C.; Balboni, E.; Baumer, T.; Treinen, K.; Kersting, A. B.; Zavarin, M. Plutonium Desorption from Nuclear Melt Glass-Derived Colloids and Implications for Migration at the Nevada National Security Site, USA. *Environ. Sci. Technol.* **2019**, *53*, 12238−12246.

https://dx.doi.org/10.1021/acsearthspacechem.0c00195
ACS Earth Space Chem. 2020, 4, 1993−2006

(59) Novikov, A. P.; Kalmykov, S. N.; Utsunomiya, S.; Ewing, R. C.; Horreard, F.; Merkulov, A.; Clark, S. B.; Tkachev, V. V.; Myasoedov, B. F. Colloid transport of plutonium in the far-field of the Mayak Production Association, Russia. *Science* **2006**, *314*, 638−641.
(60) Batuk, O. N.; Conradson, S. D.; Aleksandrova, O. N.; Boukhalfa, H.; Burakov, B. E.; Clark, D. L.; Czerwinski, K. R.; Felmy, A. R.; Lezama-Pacheco, J. S.; Kalmykov, S. N.; Moore, D. A.; Myasoedov, B. F.; Reed, D. T.; Reilly, D. D.; Roback, R. C.; Vlasova, I. E.; Webb, S. M.; Wilkerson, M. P. Multiscale Speciation of U and Pu at Chernobyl, Hanford, Los Alamos, McGuire AFB, Mayak, and Rocky Flats. *Environ. Sci. Technol.* **2015**, *49*, 6474−6484.
(61) Lukashenko, S.; Kabdyrakova, A.; Lind, O. C.; Gorlachev, I.; Kunduzbayeva, A.; Kvochkina, T.; Janssens, K.; De Nolf, W.; Yakovenko, Y.; Salbu, B. Radioactive particles released from different sources in the Semipalatinsk Test Site. *J. Environ. Radioact.* **2020**, *216*, 106160.
(62) Joshi, S. R. Lanthanum fluoride coprecipitation techniques for the preparation of actinides for alpha-spectrometry. *J. Radioanal. Nucl. Chem.* **1985**, *90*, 409−414.
(63) Hayes, T. M.; Boyce, J. B. Extended X-Ray Absorption Fine Structure Spectroscopy. In *Solid State Physics*, Ehrenreich, H., Seitz, F., Turnbull, D., Eds.; Academic Press, 1983; Vol. *37*, pp 173−351.
(64) Booth, C. H. *RSXAP EXAFS Analysis Package*. 2012. http://lise.lbl.gov/RSXAP/ (accessed 2020-10-09).
(65) Li, G. G.; Bridges, F.; Booth, C. H. X-ray absorption fine-structure standards - A comparison of experiment and theory. *Phys. Rev. B: Condens. Matter Mater. Phys.* **1995**, *52*, 6332−6348.
(66) Ankudinov, A. L.; Ravel, B.; Rehr, J. J.; Conradson, S. D. Real-space multiple-scattering calculation and interpretation of x-ray-absorption near-edge structure. *Phys. Rev. B: Condens. Matter Mater. Phys.* **1998**, *58*, 7565−7576.
(67) Booth, C. H.; Hu, Y. J. Confirmation of standard error analysis techniques applied to EXAFS using simulations. *Proceedings of 14th International Conference on X-Ray Absorption Fine Structure (XAFS14)*, 2009; p 190.
(68) Wyckoff, R. W. G. *Crystal Structures*; Interscience Publishers: New York, 1963.
(69) Wylie, E. M.; Olive, D. T.; Powell, B. A. Effects of Titanium Doping in Titanomagnetite on Neptunium Sorption and Speciation. *Environ. Sci. Technol.* **2016**, *50*, 1853−1858.
(70) Romanchuk, A. Y.; Kalmykov, S. N.; Egorov, A. V.; Zubavichus, Y. V.; Shiryaev, A. A.; Batuk, O. N.; Conradson, S. D.; Pankratov, D. A.; Presnyakov, I. A. Formation of crystalline PuO2+x·nH(2)O nanoparticles upon sorption of Pu(V,VI) onto hematite. *Geochem. Cosmochim. Acta* **2013**, *121*, 29−40.
(71) Hu, Y.-J.; Kestrel Schwaiger, L.; Booth, C. H.; Kukkadapu, R. K.; Cristiano, E.; Kaplan, D.; Nitsche, H. Molecular interactions of plutonium(VI) with synthetic manganese-substituted goethite. *Radiochim. Acta* **2010**, *98*, 655.
(72) Bargar, J. R.; Reitmeyer, R.; Lenhart, J. J.; Davis, J. A. Characterization of U(VI)-carbonato ternary complexes on hematite: EXAFS and electrophoretic mobility measurements. *Geochem. Cosmochim. Acta* **2000**, *64*, 2737−2749.
(73) Seco, F.; Hennig, C.; Pablo, J. d.; Rovira, M.; Rojo, I.; Martí, V.; Giménez, J.; Duro, L.; Grivé, M.; Bruno, J. Sorption of Th(IV) onto Iron Corrosion Products: EXAFS Study. *Environ. Sci. Technol.* **2009**, *43*, 2825−2830.
(74) Dumas, T.; Guigue, M.; Moisy, P.; Colina-Ruiz, R.; Mustre de Leon, J.; Matara-Aho, M.; Solari, P. L.; Monfort, M.; Moulin, C.; Beccia, M. R.; Auwer, C. D. Experimental Speciation of Plutonium-(IV) in Natural Seawater. *Chemistryselect* **2018**, *3*, 2021−2024.
(75) Shannon, R. D. Revised Effective Ionic-Radii and Systematic Studies of Interatomic Distances in Halides and Chalcogenides. *Acta Crystallogr., Sect. A: Cryst. Phys., Diffr., Theor. Gen. Crystallogr.* **1976**, *32*, 751−767.
(76) Wang, X.; Zhu, M.; Koopal, L. K.; Li, W.; Xu, W.; Liu, F.; Zhang, J.; Liu, Q.; Feng, X.; Sparks, D. L. Effects of crystallite size on the structure and magnetism of ferrihydrite. *Environ. Sci.: Nano* **2016**, *3*, 190−202.
(77) Siroux, B.; Beaucaire, C.; Tabarant, M.; Benedetti, M. F.; Reiller, P. E. Adsorption of strontium and caesium onto an Na-MX80 bentonite: Experiments and building of a coherent thermodynamic modelling. *Appl. Geochem.* **2017**, *87*, 167−175.
(78) Vila, F. D.; Rehr, J. J.; Rossner, H. H.; Krappe, H. J. Theoretical x-ray absorption Debye-Waller factors. *Phys. Rev. B: Condens. Matter Mater. Phys.* **2007**, *76*, 014301.
(79) Stefánsson, A. Iron(III) hydrolysis and solubility at 25 degrees C. *Environ. Sci. Technol.* **2007**, *41*, 6117−6123.
(80) Cornell, R. M.; Giovanoli, R.; Schneider, W. Review of the hydrolysis of Fe(III) and the crystallization of amorphous Fe(III) hydroxide hydrate. *J. Chem. Technol. Biotechnol.* **1989**, *46*, 115−134.
(81) Downward, L.; Booth, C. H.; Lukens, W. W.; Bridges, F. A variation of the F-Test for determining statistical relevance of particular parameters in EXAFS fits. *AIP Conf. Proc.* **2007**, *882*, 129.
(82) Kaur, N.; Gräfe, M.; Singh, B.; Kennedy, B. Simultaneous incorporation of Cr, Zn, Cd and Pb in the goethite structure. *Clays Clay Miner.* **2009**, *57*, 234−250.
(83) Yang, J.-Y.; Fu, Y.-L.; Chu, J.; Ng, S. W. Goethite, alpha-FeO(OH), from single-crystal data. *Acta Crystallogr., Sect. E: Struct. Rep. Online* **2006**, *62*, m2310−m2312.
(84) *Sources Contributing to Radioactive Contamination of the Techa River and Areas Surrounding the Mayak Production Association, Urals, Russia*; Statens Straalevern: Oesteraas, Norway, 1997; p 142, http://inis.iaea.org/search/search.aspx?orig_q=RN:29032387, 82-993079-6-1.
(85) Toropov, A. S. Migration Forms of Anthropogenic Radionuclides in Tunnel Waters at the Degelen Mountains, Semipalatinsk Test Site. *Geochem. Int.* **2020**, *58*, 342−351.
(86) Berner, U. R. Evolution of pore water chemistry during degradation of cement in a radioactive waste repository environment. *Waste Manag.* **1992**, *12*, 201−219.
(87) Wallace, S. H.; Shaw, S.; Morris, K.; Small, J. S.; Burke, I. T. Alteration of Sediments by Hyperalkaline K-Rich Cement Leachate: Implications for Strontium Adsorption and Incorporation. *Environ. Sci. Technol.* **2013**, *47*, 3694−3700.
(88) Wallace, S. H.; Shaw, S.; Morris, K.; Small, J. S.; Fuller, A. J.; Burke, I. T. Effect of groundwater pH and ionic strength on strontium sorption in aquifer sediments: Implications for Sr-90 mobility at contaminated nuclear sites. *Appl. Geochem.* **2012**, *27*, 1482−1491.
(89) Deng, Y.; Harsh, J. B.; Flury, M.; Young, J. S.; Boyle, J. S. Mineral formation during simulated leaks of Hanford waste tanks. *Appl. Geochem.* **2006**, *21*, 1392−1409.
(90) Calvin, S.; Riedel, C. J.; Carpenter, E. E.; Morrison, S. A.; Stroud, R. M.; Harris, V. G. Estimating crystallite size in polydispersed samples using EXAFS. *Phys. Scr.* **2005**, *T115*, 744−748.

https://dx.doi.org/10.1021/acsearthspacechem.0c00195
ACS Earth Space Chem. 2020, 4, 1993−2006